Received: 3 May 2018 | Revised: 12 May 2020 | Accepted: 14 May 2020

DOI: 10.1002/jnm.2781

WILEY

EMF18 SPECIAL ISSUE

Hysteresis and eddy-current losses in electrical steel utilising edge degradation due to cutting effects

Silas Elfgen[1] | **Paavo Rasilo**[2] | **Kay Hameyer**[3]

[1]R&D Electrification, DENSO Automotive Deutschland GmbH, Wegberg, Germany

[2]Unit of Electrical Engineering, Tampere University, Tampere, Finland

[3]Institute of Electrical Machines, RWTH Aachen University, Aachen, Germany

Correspondence
Silas Elfgen, Friedrich-List-Allee 42, 41844 Wegberg, Germany.
Email: silas.elfgen@rwth-aachen.de, s.elfgen@eu.denso.com

Abstract

Cutting of electrical steel sheets typically deteriorates the permeability and increases the iron loss close to the cutting edges. We estimated iron losses in the cross-section of electrical steel sheets by numerically solving the 1-D and 2-D eddy-current distributions while accounting for static magnetic behaviour with a hysteresis model. The magnetization curves in the cross-section are defined using a continuous local material model, making them dependent on the distance from the cut edge by a degradation profile. Damaged and undamaged hysteresis loops were identified by measurements of different wide strips of M400-50A steel sheets. The eddy-current distributions were solved when the strips of different widths were excited with sinusoidal average flux densities at different frequencies. It was found that the cutting degradation also affects the eddy-current loss particularly around 1.0 T. The exact shape of the degradation profile was found to be less significant while the increase of excess losses is significant for the overall loss estimation.

KEYWORDS

cut edges, edge degradation, hysteresis model, iron losses, thin sheet model

1 | INTRODUCTION

Electrical steel sheets are widely used in electrical machines. The laminations are cut into the desired shape during the production process. It is well known that the processing gives rise to mechanical stresses and deformations, which deteriorate the magnetic properties of the sheets.[1-3] Due to the cutting process residual stress is introduced to the lamination particularly in the vicinity of the cut edge. This leads to a continuous local degradation of the magnetic properties.

In production, different cutting techniques are used, such as thermal cutting, for example, laser, for prototyping and mechanical cutting such as blanking in mass production. The resulting width of the magnetically degraded zone depends on the combination of processing and material specific parameters and can extend over several millimetres.[1,3-6] The effect can be measured either in terms of magnetic properties such as the flux density distribution or mechanical properties such as the microhardness.

As a consequence of the residual local stress, the magnetic permeability distribution is influenced along with the resulting local iron losses. In application with small geometrical dimensions such as a rotor or a stator tooth, the influence of the cut edges is significant and has to be considered within the description of the material properties. Moreover, the cutting influence has to be considered within the iron loss calculation of the steel lamination.

In classical frequency- or time-domain iron loss calculations, the eddy-current loss parameter is calculated analytically.[7-9] Therefore, eddy-current losses are considered to be independent from the influences of the cut edge. A 2-D

finite element (FE) model able to account for the return path of the eddy currents close to the cut edges was presented in References [1,10], but separation of hysteresis and eddy-current losses was not discussed and the frequency was limited to 50 Hz. The novel contribution in this article is the quantification of the effect of cutting on the hysteresis and eddy-current losses up to 1 kHz, accurately accounting for the distribution of the eddy currents in the lamination cross-section. Electrical steel strips of different widths are measured and simulated to analyse the effect of the cutting degradation on the losses. In the 1-D simulations, average magnetization curves measured from the strips are used as the constitutive laws and the single strips are assumed to have homogeneous material properties. In the 2-D simulations, different local material models identified from the measurements are applied for the representation of the local magnetic material degradation. Excess losses are then obtained as the difference of measured and simulated losses. The resulting loss contributions are analysed and compared for various frequencies and magnetic polarisation levels.

The article is structured as follows. A brief introduction is given discussing the magnetic characterisations for the quantification of the cutting influence on the magnetic behaviour of an exemplary silicon steel. Next, the numerical 1-D and 2-D eddy current simulations are explained along with the local material model. The applicability of the models and the resulting iron losses are discussed and compared to measurement data. Finally, a summary of the presented results is given.

2 | MAGNETIC CHARACTERISATION

Within the standard IEC60404-3, the single sheet tester (SST) offers the possibility of considering manufacturing influences within the characterisation of soft magnetic materials. Due to the larger specimen size it is possible to characterise specimens with a variety of residual stress. In this article an SST with a basic specimen size of 120 mm × 120 mm is used.

A standard iron steel of the grade M400-50A is selected for the presented study. The basic specimens are cut into 2 × 60 mm, 4 × 30 mm, 6 × 20 mm, 12 × 10 mm and 24 × 5 mm strips along the rolling direction (RD) using guillotine shear resulting into mechanical residual stress and plastic strain close to the cutting surface. The width of the strips is denoted by variable w. The applied flux during the characterisation is always in parallel to the cut surface. The material characterisations are conducted in accordance with the standard IEC60404-3 under sinusoidal flux-density conditions.

The resulting magnetization curves and the corresponding losses are depicted in Figure 1 at 50 Hz. With decreasing strip width the deterioration of the material becomes apparent. In terms of the magnetization curves, depicted in Figure 1A, a shearing of the branches follows as a consequence of the increased residual stress. While the coercive field strength increases, a reduction in the remanent flux density can be seen. This leads to a significant increase in total measured iron losses in smaller specimen sizes, as depicted in Figure 1B.

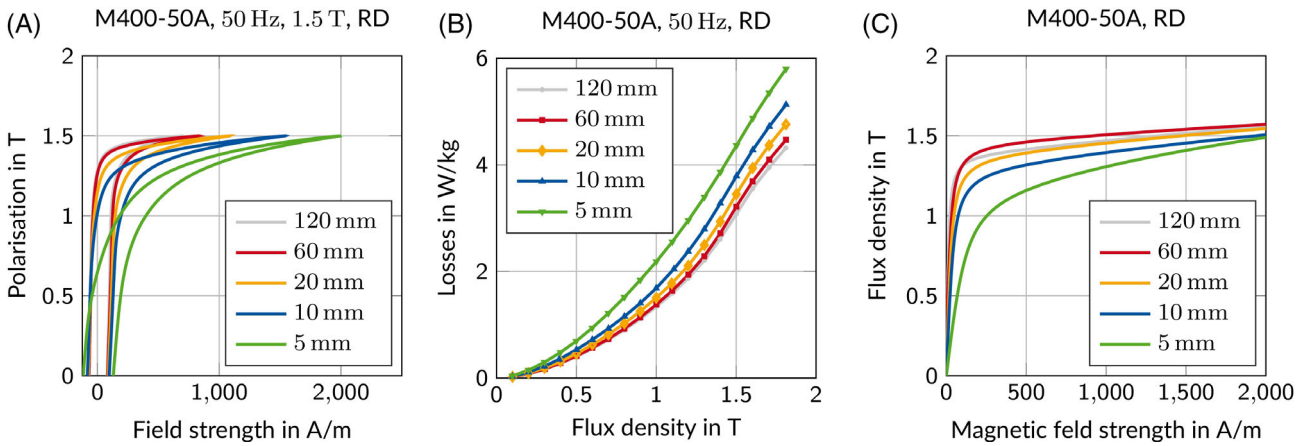

FIGURE 1 A, Measured magnetization curves at 1.5 T. B, Corresponding specific losses of different specimen widths w both at 50 Hz with external field applied in rolling direction. C, The measured anhysteretic behaviour extracted from quasi-static measurements

3 | METHODS

3.1 | 1-D eddy current simulation

The first model used to study the effect of cut edges on eddy currents is a 1-D mesh-free (MF) model presented in References [11,12]. It is a time dependent 1-D lamination model describing the penetration of the electromagnetic field into a sheet of thickness d and electrical conductivity σ according to

$$\frac{\partial^2 H(z,t)}{\partial z^2} = \sigma \frac{\partial B(z,t)}{\partial t}, \tag{1}$$

where $B(z,t)$ and $H(z,t)$ represent the local flux-density and field distributions across the sheet thickness $z \in \left[-\frac{d}{2}, \frac{d}{2}\right]$. The MF model reduces the number of unknowns and decreases the necessary simulation time in comparison to a FE-solution. In this model the flux density distribution $B(z,t)$ is approximated using a truncated Fourier cosine series with N_b terms, denoting the amplitudes of the space harmonics as $B_n(t)$:

$$B(z,t) = \sum_{n=0}^{N_\mathrm{b}-1} B_n(t)\alpha_n(z), \quad \alpha_n(z) = \cos\left(2n\pi\frac{z}{d}\right). \tag{2}$$

To satisfy (1) in the strong sense, the field strength is expressed as

$$\tilde{H}(z,t) = H_\mathrm{s}(t) - \sigma d^2 \sum_{n=0}^{N_\mathrm{b}-1} \frac{\partial B_n(t)}{\partial t}\beta_n(z) \tag{3}$$

where H_s is the field strength on the surface of the sheet. The local function $\beta_n(z)$ is defined to comply with the boundary conditions of $\beta_n(\pm d/2) = 0$ and $\alpha_n(z) = -d\partial^2\beta_n(z)/\partial z^2$ as written in Reference [12]. By requiring the error between $\tilde{H}(z,t)$ and the actual field strength $H(B(z,t))$ obtained from the constitutive material law to be zero in the weak sense with respect to the basis functions, the equation system

$$\begin{bmatrix} H_\mathrm{s}(t) \\ 0 \\ \vdots \end{bmatrix} = \frac{1}{d}\int_{-d/2}^{d/2} H(B(z,t)) \begin{bmatrix} \alpha_0(z) \\ \alpha_1(z) \\ \vdots \end{bmatrix} dz + \sigma d^2 \mathbf{C} \frac{\partial}{\partial t} \begin{bmatrix} B_0(t) \\ B_1(t) \\ \vdots \end{bmatrix} \tag{4}$$

is obtained, $\mathbf{C}$ being a constant matrix resulting from the integrations of the products $\alpha_m(z)\beta_n(z)$ over the sheet thickness $z \in \left[-\frac{d}{2}, \frac{d}{2}\right]$.[12] This system describes the relationship between the surface field strength $H_s(t)$ and the average flux density $B_0(t)$, which result from the characterisation at the SST. The electrical conductivity of the studied material is $\sigma = 2.07\,\mathrm{MSm}$.

With the aim to consider the material deterioration in the eddy current simulation, the corresponding anhysteretic behaviour $H(B)$ has to be used in the mesh free model in (4). For a strip of width w, these properties can be either measured or calculated using the parametrised continuous local cut edge model published in Reference [13]. In this article the anhysteretic material properties for width w are derived from measurements under quasi-static field conditions, using the SST described above. The resulting magnetization characteristics of the different strip widths are depicted in Figure 1C.

With increasing deterioration a shearing of the hysteresis curves and hence the anhysteretic behaviour can be observed. In Figure 2, measurement and simulation results are presented at a high frequency for the skin effect to be present. Thereby, the influence of the deterioration on the eddy current distribution in the lamination can be demonstrated as follows. Figure 2A shows measured and resulting simulated magnetization curves of the undamaged material at 750 Hz and 1.0 T. The measured surface field strength H_meas contains magnetic field contributions, which are the static hysteresis field H_DC, the eddy current field H_eddy and the excess field H_ex. The resulting simulated field H_sim consists of the measured static hysteresis field H_DC and the eddy current field $H_\mathrm{eddy,mf}$ resulting from the mesh free model.

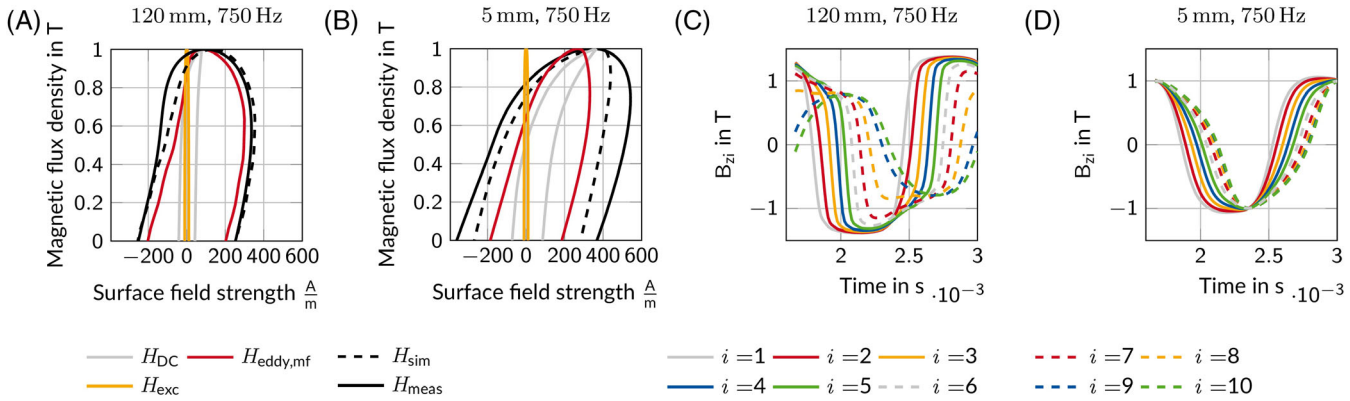

FIGURE 2 A, Measured and simulated magnetization curves $B(H)$. B, Corresponding local flux density loci $B_{z,i}$ at equidistant locations i across the lamination, for different shear cut specimen widths w, both at 750 Hz and 1.0 T

In Figure 2B the magnetization behaviour of a deteriorated specimen of 5 mm is depicted under equal maximum flux density and frequency. A significant increase in magnetising current is noticeable, which is caused by the increased static hysteresis field and the excess field contribution.

The reduced differential susceptibility of the deteriorated material leads to a reduction in the change of the magnetic field with a change in the flux density. The resulting local flux density distribution across the lamination of an uncut and shear cut specimen can be seen in Figure 2C,D, respectively. The lamination is subdivided into 10 equidistant layers. In the shear cut lamination a damping of the skin effect caused by the sheared anhysteretic properties becomes apparent at high frequencies. While in the undamaged lamination, the skin effect strongly influences the flux density amplitude between outer surface layer $i = 1$ or $B_{z,1}$ and centre layer $i = 10$ or $B_{z,10}$ the effect especially in the amplitude is less pronounced considering the specimen of 5 mm.

3.2 | Identification of degradation profile and magnetization curves

In order to cope with local magnetic properties it is necessary to continuously model the resulting magnetic degradation effect. Therefore, a continuous local material model is used, following the approach presented in References [13-15]. The relationship between the magnetic flux density B and field strength H is made dependent on the distance x from the cut edge. This dependency is expressed as

$$B(H,x) = B_{\mathrm{un}}(H)(1-\eta(x)) + B_{\mathrm{dam}}(H)\eta(x), \tag{5}$$

where $B_{\mathrm{un}}(H)$ is the magnetization curve of the undamaged material and $B_{\mathrm{dam}}(H)$ is the magnetization curve right at the damaged edge. The expression is derived from the model presented in Reference [13]. Function $\eta(x)$ is called a degradation profile, and it defines how the degradation extends into the material. In this work, three degradation profiles are considered: a constant (0th order), a linear (first) and a quadratic (second) profile. These are defined, respectively, as

$$\eta(x) = \begin{cases} 1 \ \forall \ 0 \le x \le \delta \\ 0 \ \forall \ x > \delta, \end{cases} \tag{6}$$

$$\eta(x) = \begin{cases} 1 - \dfrac{x}{\delta} \ \forall \ 0 \le x \le \delta \\ 0 \quad\ \forall \ x > \delta, \end{cases} \tag{7}$$

$$\eta(x) = \begin{cases} 1 - \dfrac{2x}{\delta} + \left(\dfrac{x}{\delta}\right)^2 \forall \ 0 \le x \le \delta \\ 0 \qquad\qquad\ \forall \ x > \delta, \end{cases} \tag{8}$$

where δ corresponds to the maximum distance at which the degradation appears. The constant profile represents a sliced model, as for example, used in Reference [5], with a damaged area at each side of the specimen and the unaffected material in the centre. The quadratic profile is derived from microhardness measurements and used within the continuous local material model in Reference [13]. It provides a smooth transition in the material properties from the damaged region to the undamaged region so that $\eta'(\delta) = 0$. Averaging the flux density (5) over half of the sample width w gives

$$B_{\mathrm{av}}(H,w) = \frac{2}{w}\int_0^{w/2} B(H,x)dx = B_{\mathrm{un}}(H)(1-\eta_{\mathrm{av}}(w)) + B_{\mathrm{dam}}(H)\eta_{\mathrm{av}}(w), \tag{9}$$

where

$$\eta_{\mathrm{av}}(w) = \frac{2}{w}\int_0^{w/2} \eta(x)dx = \frac{2}{w}\left[y - \frac{y^2}{\delta} + \frac{y^3}{3\delta}\right], \quad \text{with } y = \min\left(\frac{w}{2},\delta\right) \tag{10}$$

is the average of the degradation profile.

The relationships $B_{\mathrm{unun}}(H)$ and $B_{\mathrm{damdam}}(H)$ are hysteretic and need to be estimated from the measurements together with the influence depth δ. The $B(H)$ curves measured at frequency of 10 Hz and amplitude of $B_{\max} = 1.8$ T from samples of different widths are used for the fitting. The undamaged curve $B_{\mathrm{unun}}(H)$ is taken equal to that measured from the 120 mm sheet. Following the idea of Reference [16], the ascending branch of the damaged curve $B_{\mathrm{damdam}}(H)$ is expressed analytically as

$$B_{\mathrm{asc,dam}}(H) = B_{\max}\frac{2g(H) - g(H_{\max}) - g(-H_{\max})}{g(H_{\max}) - g(-H_{\max})}, \tag{11}$$

where $H_{\max} = 9780$ A m^{-1} is the field strength value corresponding to $B_{\max}$, and which is taken equal to that of the undamaged curve, since the saturation should not be affected by the cutting. Function $g(H)$ is written as

$$g(H) = \begin{cases} \dfrac{H + h_{\mathrm{c}}}{h_1 + k_1|H + h_{\mathrm{c}}|} & \forall\ H \le -h_{\mathrm{c}} \\ \dfrac{H + h_{\mathrm{c}}}{h_1 + k_2|H + h_{\mathrm{c}}|} & \forall\ H > -h_{\mathrm{c}} \end{cases}, \tag{12}$$

where h_c, h_1, k_1 and k_2 are fitting parameters. The five parameters δ, h_c, h_1, k_1 and k_2 are estimated by least-squares fitting by comparing the average hysteresis loops (9) with those measured from w = 5, 10, 20 and 60 mm sheets (Figure 1A). The obtained undamaged and damaged magnetization curves are shown in Figure 3A for the quadratic degradation profile. The hysteresis curves and losses in different sample widths obtained using the fitted curves are compared with the measurements in Figure 3B,C, respectively. The fitting errors are calculated as $\|\boldsymbol{m} - \boldsymbol{s}\|/\|\boldsymbol{m}\|$, where vectors $\boldsymbol{m}$ and $\boldsymbol{s}$, respectively, contain the measured and simulated data point values for the flux density and hysteresis loss. In the case of the constant, linear and quadratic profiles, the flux-density errors are 7.0%, 7.1% and 7.4% and hysteresis loss errors are 0.76%, 0.61% and 0.78%, indicating a reasonable correspondence between the simulations and measurements. For the constant, linear and quadratic profiles, the values obtained for δ were 1.73, 3.48 and 5.09 mm, respectively. Parameter δ increases when the profile order increases, since the faster decrease requires a larger deterioration width in order to produce the same average η_{av}.

3.3 | 2-D eddy current simulation

In the 1-D model, homogeneous material properties corresponding to the average flux-densities (9) for different w were assumed. In order to model the effect of the local degradation on the eddy-current distribution in the sample, a 2-D

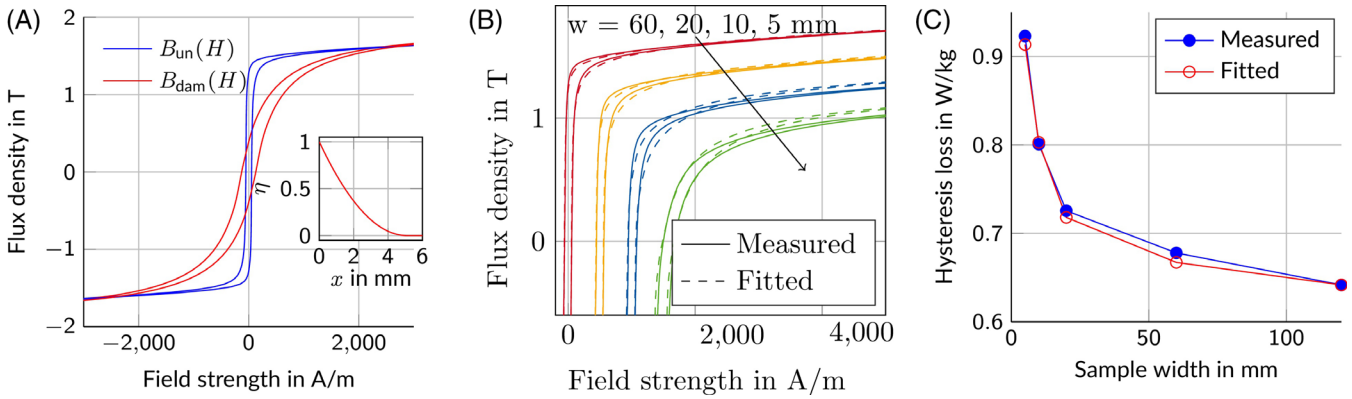

FIGURE 3 A, Identified magnetization curves $B_{un}(H)$ and $B_{dam}(H)$ and degradation profile $\eta(x)$. B, Measured and fitted magnetization curves in different samples both at 10 Hz. The ones at 10, 20 and 60 mm are shifted from the origin for clarity. C, Measured and fitted hysteresis losses in different samples at 10 Hz

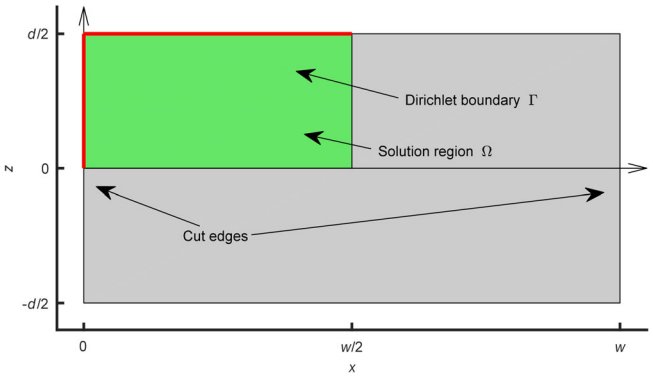

FIGURE 4 Problem definition for the 2-D FE problem

model is developed. Consider the sample to be placed in the xz-plane according to Figure 4, such that $x = 0$ corresponds to the left cut edge. Unit vectors are denoted $\boldsymbol{x}$, $\boldsymbol{y}$ and $\boldsymbol{z}$. For symmetry reasons, only the top left quarter Ω and its outer boundary Γ need to be considered. When a time-varying flux density $\boldsymbol{B} = B(x, z, t)\boldsymbol{y}$ flows through the sheet perpendicularly to the cross-section, a current density $\boldsymbol{J} = J_x(x, z, t)\boldsymbol{x} + J_z(x, z, t)\boldsymbol{z}$ is induced into the cross-sectional plane according to Faraday's law. Since the eddy-current density is divergence free, it can be expressed as the curl of the magnetic field strength $H = H(x, z, t)\boldsymbol{y}$:

$$\boldsymbol{J}(x,z,t) = \nabla \times [H(x,z,t)\boldsymbol{y}]. \tag{13}$$

The 2-D eddy-current problem becomes

$$-\frac{1}{\sigma}\nabla\cdot\nabla H(x,z,t) + \frac{\partial B(x,z,t)}{\partial t} = 0, \tag{14}$$

where H is used as the field variable to be solved.

The relationship between B and H is determined by the scalar relationship (5), where $B_{un}(H)$ and $B_{un}(H)$ are modelled with the hysteresis model of Reference [17], which takes as input parameters the ascending branches of the hysteresis loops which were identified from the measurements. However, the model of Reference [17] is an inverse model implemented in the form $H = H_{hy}(B)$ instead of $B = B_{hy}(H)$. In addition, we want to impose an integral condition for B in order to force the desired average flux density $B_{av}(t)$ through the sheet. We thus choose B_{un} and B_{dam} as additional variables in addition to H. The total equation system to be solved in Ω becomes

$$-\frac{1}{\sigma}\nabla\cdot\nabla H(x,z,t)+\frac{\partial}{\partial t}[B_{\mathrm{un}}(x,z,t)(1-\eta(x))+B_{\mathrm{dam}}(x,z,t)\eta(x)]=0, \tag{15}$$

$$H_{\mathrm{hy,un}}(B_{\mathrm{un}}(x,z,t))-H(x,z,t)=0, \tag{16}$$

$$H_{\mathrm{hy,dam}}(B_{\mathrm{dam}}(x,z,t))-H(x,z,t)=0, \tag{17}$$

$$\frac{4}{wd}\int_{\Omega}[B_{\mathrm{un}}(x,z,t)(1-\eta(x))+B_{\mathrm{dam}}(x,z,t)\eta(x)]d\Omega=B_{\mathrm{av}}(t). \tag{18}$$

Solving this system forces the outputs of the undamaged and damaged hysteresis models $H_{\mathrm{hy,un}}$ and $H_{\mathrm{hy,dam}}$ to be equal to H used as the field variable. When this condition is met, B_{un} and B_{dam} correctly represent the two components, from which the local flux density is superposed according to (5). As a boundary condition, H is required to be constant at Γ. Equation (15) is discretised using the Galerkin method with nodal shape functions for H, and B_{un} and B_{dam} are evaluated in the Gauss integration points. After the FE solution has been obtained, the time- and space-averaged eddy-current and hysteresis loss densities (in Wm^{-3}) are calculated as

$$p_{\mathrm{cl}}=\frac{4}{wdT}\int_0^T\int_{\Omega}\frac{1}{\sigma}\|\mathbf{J}(x,z,t)\|^2 d\Omega \tag{19}$$

$$p_{\mathrm{hy}}=\frac{4}{wdT}\int_0^T\int_{\Omega}H(x,z,t)\frac{\partial}{\partial t}[B_{\mathrm{un}}(x,z,t)(1-\eta(x))+B_{\mathrm{dam}}(x,z,t)\eta(x)]d\Omega, \tag{20}$$

respectively.

In Figure 5 the resulting local flux density and current density distributions on the simulated lamination area are presented for an undamaged sample in the top row and a damaged sample in the bottom row. The influence of the cut edge on the local field distribution can be seen in terms of reduced local flux density and pushing the edge effect of the local current density deeper in to the material.

4 | COMPARISON OF RESULTING LOSS ESTIMATION

The iron losses calculated from the 1-D and 2-D eddy current simulation are now discussed and compared with measurements. As mentioned previously, classical eddy current losses are usually considered to be unaffected by the cut edges, as the parameters of the analytical description are not influenced by residual stress as a consequence of the cutting procedure. The analytical classical eddy-current loss estimation is done using $p_{\mathrm{cl}}\propto\sigma d^2$ neglecting the skin effect[8] or considering it by an additional loss contribution.[8] In the simulations with the 1-D and 2-D models, the eddy-current losses become dependent on the degraded material properties due to the consideration of the skin effect.

In Figure 6 the resulting iron loss components are presented in an exemplary working point at 1 kHz and 1.4 T, comparing the 1-D and 2-D simulation results at different sheet widths. The losses in 2-D are calculated using different degradation profile orders to account for the local deterioration. As seen in Figure 6 the resulting hysteresis and eddy-current losses have a small sensitivity towards the deterioration profile. Hence, the resulting calculated loss contributions in 2-D vary little with the order of the deterioration profile. The hysteresis losses used in the 1-D model represent the actual measured hysteresis losses. The accordance between the 1-D and 2-D hysteresis losses in Figure 6 proves the accuracy of the hysteresis loss estimation by the 2-D model, as also demonstrated in Figure 3C.

When comparing 1-D and 2-D simulation results in Figure 6, both hysteresis and eddy-current losses show similar trends as functions of the strip width. In both cases, decreasing eddy-current loss is observed with decreasing strip width. This is due to increased magnetic skin depth as well as the reduced differential permeability caused by the residual stress.

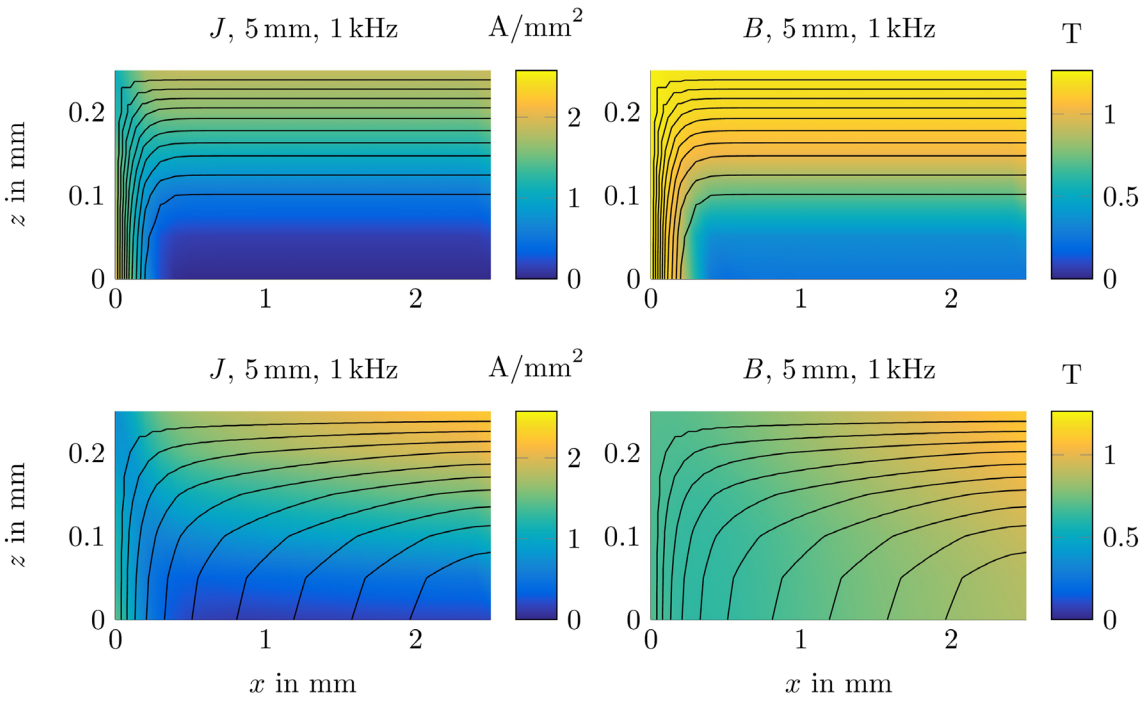

FIGURE 5 Simulated rms eddy current density J (left column) and rms flux density B (rigth column) of undamaged (top line) and damaged lamination (bottom line) at an average flux density of 1.0 T

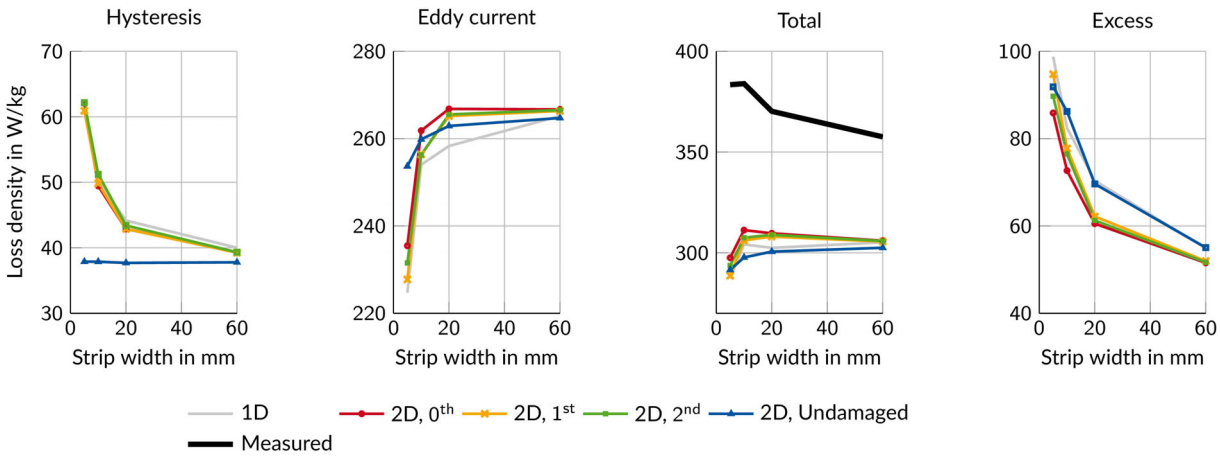

FIGURE 6 Comparison of the iron loss components at 1 kHz and 1.4 T (from left to right): Measured hysteresis loss in 1-D case vs modelled hysteresis losses in 2-D case considering different degradation profiles; calculated eddy-current losses for 1-D and 2-D cases; the resulting measured iron losses vs the 1-D and the 2-D case excluding the excess contribution; and the remaining excess losses for all cases

The difference between the measured losses and the simulated hysteresis and eddy-current losses is assumed to represent excess losses. Figure 7A shows this difference as a function of the frequency calculated using the 1-D and 2-D simulation results. The resulting shape follows the well-known behaviour $p_{ex} \propto f^{0.5}$ of the excess losses,[8] which verifies the assumption. The excess losses increase when the strip width decreases. Furthermore, the difference between the losses of the 1-D and 2-D simulation also decreases with decreasing strip width.

In Figure 7A the relative share of the excess losses of the total losses at different frequencies depending on the strip width is presented. The induced residual stress acts as pinning points for the domain wall motion. Hence, it can be seen that the relative share increases in both methods up 25% with respect to the measured losses.

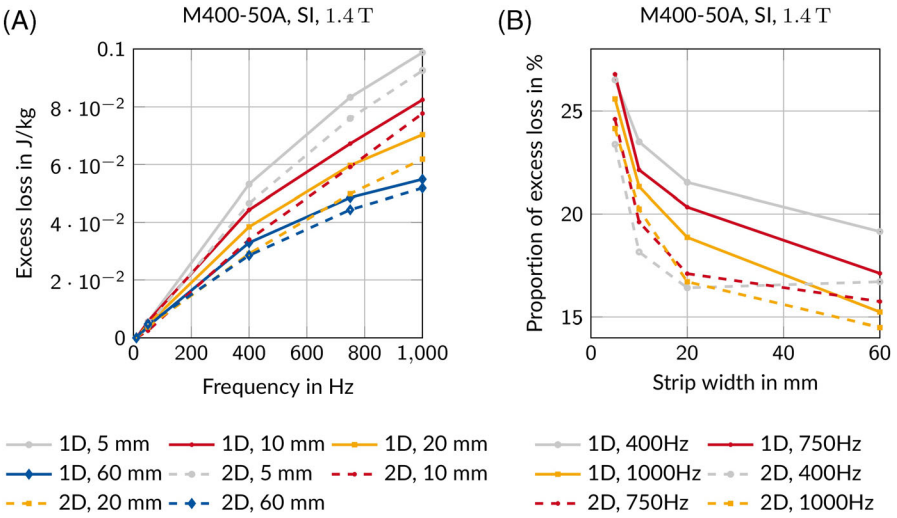

FIGURE 7 Resulting calculated excess losses vs, A, frequency and, B, strip width from 1-D and 2-D simulation considering the second order

5 | CONCLUSIONS

The effect of different material degradation models on hysteresis and eddy-current losses in shear-cut laminations was studied. Based on the small differences between the 2-D loss simulation results with different degradation profile orders, the profile shape does not significantly affect the average eddy-current losses. In addition, the 1-D model that utilises the average magnetization properties measured for each strip width produced losses rather closely to the 2-D model, in which the local degradation profile was used. This implies that despite the rather significant effect of the degradation on the eddy-current distribution in Figure 5, the total eddy-current loss is not significantly affected by the edge effect. This is a positive result, since implementing the 1-D model is relatively simple and its computational burden is lower than that of the 2-D model. However, modelling the skin effect along the lamination thickness is important because this is the only mechanism through which the magnetization properties affect the eddy-current distribution in the 1-D model.

As a proposal for future work, the 2-D model could be used for modelling a stack of two laminations whose edges are in galvanic contact due to cutting burrs. It might be interesting to study how the increased edge effect in the damaged sheets would change the eddy-current distribution in the stack and losses due to the contacts. Previous research also implies that the effect of hysteresis on the magnetic field and eddy-current distributions is rather small,[18,19] and thus hysteresis could be considered only in the postprocessing stage to simplify the models.

Excess losses, defined as the difference between measured and simulated losses, were found to behave approximately according to the statistical loss theory. It was found that in the 5 mm laminations, the excess losses can comprise more than one-fourth of the total iron loss, making prediction of the losses difficult. This is especially relevant, when losses in narrow regions such as tooth tips of electrical machines are to be analysed.

ORCID

Silas Elfgen https://orcid.org/0000-0002-5233-7540
Paavo Rasilo https://orcid.org/0000-0002-0721-5800

REFERENCES

1. Crevecoeur G, Sergeant P, Dupre L, Vandenbossche L, Walle R. Analysis of the local material degradation near cutting edges of electrical steel sheets. *IEEE Trans Magn*. 2008;44(11):3173-3176.
2. Schoppa A, Schneider J, Wuppermann C-D. Influence of the cutting process on the magnetic properties of non-oriented electrical steels. *J Magn Magn Mater*. 2000;215-216:100-102.
3. Siebert R, Wetzig A, Beyer E, Betz B, Grunzweig C, Lehmann E. Localized investigation of magnetic bulk property deterioration of electrical steel: Analysing magnetic property drop thorough mechanical and laser cutting of electrical steel laminations using neutron grating interferometry. *Proceedings of the 3rd International Electric Drives Production Conference (EDPC)*. New York, NY: IEEE; 2013:1-5.
4. Baudouin P, De Wulf M, Kestens L, Houbaert Y. The effect of the guillotine clearance on the magnetic properties of electrical steels. *J Magn Magn Mater*. 2003;256(1-3):32-40.

5. Gmyrek Z, Cavagnino A. Analytical method for determining the damaged area width in magnetic materials due to punching process. *Proceedings of the 37th Annual Conference on IEEE Industrial Electronics Society, IECON*. New York, NY: IEEE; 2011:1764-1769.
6. Maurel V, Ossart F, Billardon R. Residual stresses in punched laminations: phenomenological analysis and influence on the magnetic behavior of electrical steels. *J Appl Phys*. 2003;93(10):7106-7108.
7. Steentjes S, von Pfingsten G, Hameyer K. An application-oriented approach for consideration of material degradation effects due to cutting on iron losses and magnetizability. *IEEE Trans Magn*. 2014;50(11):416-417.
8. Bertotti G. General properties of power losses in soft ferromagnetic materials. *IEEE Trans Magn*. 1988;24(1):621-630.
9. Vandenbossche L, Jacobs S, Jannot X, McClelland M, Saint-Michel J, Attrazic E. Iron loss modelling which includes the impact of punching, applied to high-efficiency induction machines. *Proceeding of the 3rd International Electric Drives Production Conference (EDPC)*. New York, NY: IEEE; 2013:1-10.
10. Crevecoeur G, Dupre L, Vandenbossche L, Walle R. Local identification of magnetic hysteresis properties near cutting edges of electrical steel sheets. *IEEE Trans Magn*. 2008;44(6):1010-1013.
11. Gyselinck J, Sabariego RV, Dular P. A nonlinear time-domain homogenization technique for laminated iron cores in three-dimensional finite-element models. *IEEE Trans Magn*. 2006;42(4):763-766.
12. Rasilo P, Dlala E, Fonteyn K, Pippuri J, Belahcen A, Arkkio A. Model of laminated ferromagnetic cores for loss prediction in electrical machines. *IET Electr Power Appl*. 2011;5(7):580-588.
13. Elfgen S, Steentjes S, Böhmer S, Franck D, Hameyer K. Continuous local material model for cut edge effects in soft magnetic materials. *IEEE Trans Magn*. 2016;52(5):1-4.
14. Elfgen S, Steentjes S, Böhmer S, Franck D, Hameyer K. Influences of material degradation due to laser cutting on the operating behavior of PMSM using a continuous local material model. *IEEE Trans Indus Appl*. 2017;53(3):1978-1984.
15. Vandenbossche L, Jacobs S, Henrotte F, Hameyer K. Impact of cut edges on magnetization curves and iron losses in e-machines for automotive traction. *World Electr Veh J*. 2010;4(3):587-596.
16. Roshen W. Ferrite Core loss for power magnetic components design. *IEEE Trans Magn*. 1991;27(6):4407-4415.
17. Zirka SE, Moroz YI, Harrison RG, Chiesa N. Inverse hysteresis models for transient simulation. *IEEE Trans Power Deliv*. 2014;29(2):552-559.
18. Dlala E, Belahcen A, Arkkio A. On the importance of incorporating iron losses in the magnetic field solution of electrical machines. *IEEE Trans Magn*. 2010;46(8):3101-3104.
19. Rasilo P, Belahcen A, Arkkio A. Importance of iron-loss modeling in simulation of wound-field synchronous machines. *IEEE Trans Magn*. 2012;48(9):2495-2504.

How to cite this article: Elfgen S, Rasilo P, Hameyer K. Hysteresis and eddy-current losses in electrical steel utilising edge degradation due to cutting effects. *Int J Numer Model*. 2020;33:e2781. https://doi.org/10.1002/jnm.2781